Noname manuscript No.
(will be inserted by the editor)

Transient characterization of the reattachment of a massively separated turbulent boundary layer under flow control

C. Raibaudo · M. Stanislas · F. Kerhervé

Received: date / Accepted: date

Abstract

The transient dynamics of a high Reynolds number separated flow submitted to pulsed fluidic control is investigated. A spanwise array of 22 round jets, located upstream of the flap leading edge, is used as actuators to generate co-rotating structures. Simultaneous measurements of wall friction using hot-film anemometry and phase-averaged velocity using 2D2C PIV are conducted. The PIV plane contains the incoming boundary layer upstream the flap leading edge, the separation bubble and the natural reattachment region. The dynamics of the separated flow is studied under successive sequences of pulsed actuation. Pockets of turbulence are periodically generated by the separation process and pushed downstream. After the transition period, the controlled flow shows large amplitude oscillations around a steady mean, particularly for the separation area. The transient dynamics of the flow at the actuation activation is also studied. The separated flow is strongly modified by the actuation from the first pulse. Characteristic times of the transient dynamics can be determined by fitting a first-order model with delay on the data. For the reattachment, characteristic rising time $\tau_r^+ = \tau_r\ U_0\ /\ L_{sep}$ are 11.7 for the friction gain, 4.8 for the separation length and 4.1 using a Conditional Proper Orthogonal Decomposition analysis of the phase-averaged velocity fields. These values are in fairly good agreement with the previous studies on the transient reattachment and allows a more precise modeling of the process and its closed-loop control.

C. Raibaudo
Department of Mechanical and Manufacturing Engineering
Schulich School of Engineering, University of Calgary, Calgary, Canada
E-mail: cedric.raibaudo@gmail.com

M. Stanislas
École Centrale de Lille
Cité Scientifique, 59651 Villeneuve d'Ascq Cedex, France
E-mail: michel.stanislas@ec-lille.fr

F. Kerhervé
Institut PPRIME, CNRS - Université de Poitiers - ENSMA
CEAT, 43 rue de l'Aérodrome, 86036 Poitiers Cedex, France
E-mail: franck.kerherve@univ-poitiers.fr

List of symbols

A_{sep}	Area of the separation bubble
$< c_\mu >$	Transient momentum coefficient $< c_\mu >= DC\ (N_j \rho_j U_j^2 S_j)\ /\ (0.5 \rho_0 U_0^2 \delta \lambda)$
DC	Duty cycle
$E - E_0$	Friction gain (E_0 friction of the flow without control)
f	Frequency of actuation
f_{PIV}	Frequency of phase-averaging PIV
F^+	Reduced frequency of actuation $F^+ = f\ L_{sep}\ /\ U_0$
F^+_{opt}	Reduced optimum frequency of actuation $F^+_{opt} = f_{opt}\ L_{sep}\ /\ U_0$
k	Turbulent kinetic energy $k = \frac{1}{2}(u'^2 + v'^2)$
$\widehat{k}$	Phase-averaged turbulent kinetic energy
L_{sep}	Length of the separation bubble
N_c	Number of cycles used for the phase-averaging procedure
n_θ	Number of phases during the transition
Re_θ	Reynolds number based on θ
St	Strouhal number $St = f\ L_0\ /\ U_0$
t^*	Reduced time $t^* = t\ U_0\ /\ H_s$
t_d	Delay time
U_{mean}, V_{mean}	Mean streamwise and wall-normal velocity for the separated flow
$\widehat{U}, \widehat{V}$	Phase-averaged mean streamwise and wall-normal velocity
U_j	Mean velocity of the jets
U_0	Reference freestream velocity of the flow at the leading edge
VR	Velocity ratio of the jets $U_j\ /\ U_0$
x_R	Position of the reattachment point
x_S	Position of the separation point
ΔX_{vg}	Distance between the vortex generators jets and the separation line
α	Angle of the jets (around z-axis)
β	Angle of the jets (around x-axis)
δ	Boundary layer thickness
λ	Span distance between two consecutive jets
χ	Backflow function
ϕ	Diameter of the jets
τ_r, τ_s	Characteristic reattachment/separation time
τ_r^+, τ_s^+	Reduced characteristic reattachment/separation time $\tau_\star^+ = \tau_\star\ U_0\ /\ L_{sep}$
θ	Momentum thickness of the boundary layer

1 Introduction

For a few decades, turbulent boundary layers encountering separation have gain interest from both scientific and industrial communities. When aerodynamic performances are concerned, flow separation is a real issue as it can lead to severe drag penalty with related energy cost, drop of lift, or loss of control of the device (Gad-el hak (2000)), while opening fundamental questions on the intrinsic mechanisms involved in the separation process.

For the applications concerned here (typically flow around an airfoil), the flow just upstream of the separation can be subject to small or even large perturbations possibly leading to significantly different dynamics. Recently, Marquillie and Ehrenstein (2003) have suggested that the process of separation may be connected with absolute instability of the flow upstream of the separation region. The separation process is thus very sensitive to minor upstream disturbances. Avoiding separation despite any unsteady perturbations requires time-varying control strategies which adapt the actuation to variations of the parameters defining the flow state. This excludes of course passive control (generally based on solid objects introduced in the flow such as riblets or vortex generators (VG)) from the range of possible technologies.

For application prospects, actuators which can at least be turned on and off are required. Extensive research in the literature show that, when replacing passive actuators by fluidic active VG jets, better control efficiency can be achieved (Compton and Johnston (1992), Tilmann et al (2006)). In addition, these offer potentially more flexible operational characteristics. The most important drawback is the increase of energy consumption since energy supply is required. Comprehensive parametric analysis conducted by few authors (Selby et al (1992), Tilmann et al (2006), Godard et al (2006), Cuvier (2012)) on fluidic VG jets have led to optimal arrangements for efficient and robust control. When the jet is inclined to the wall and to the incoming baseline flow, two counter-rotating vortices are initially created just downstream of the device. These vortices evolve rapidly into an enhanced single coherent vortex of one sign accompanied by a much smaller and weaker region of circulation of the opposite sign near the wall. When an array of such jets are used and arranged along a spanwise line, a corresponding array of streamwise vortices is generated, forcing the flow to more or less reattach depending on the amount of momentum introduced. Different shapes of jets exit geometry have been examined (Godard et al (2006), McManus et al (1994), Tilmann et al (2006)) and key parameters have been identified thanks to extensive parametric studies. Among these parameters, the ratio of jets velocity to freestream velocity (VR) and the ratio ϕ / δ of the jet diameter to the boundary layer thickness before separation, were found to scale the strength of the induced vortex (Tilmann et al (2006) among others) and the power consumption of the VGs. If strong streamwise vortex structure may maximize the control efficiency, high VR may also results in the generation of a vortical structure away from the wall, resulting in a drop of control efficiency. Typical values of VR between 2.5 and 3 seems to offer a compromise between energy cost and control efficiency (Selby et al (1992), Lögdberg (2008)). Among the other parameters, the jet penetration which depends on the pitch angle β, is found to drive the strength of the main induced vortex generated. When the center of this vortex moves away from the wall, the control efficiency drops significantly (Milanovic and M. Q. Zaman (2004)) and optimal values of β in the range of 15° to 45° are generally reported (Selby et al (1992), Godard and Stanislas (2006)). The skew angle α, which represents the azimuthal angle between the freestream and the projection of the jets axis on the wall and which drives the symmetry of the counter-rotating vortex pair generated by a wall normal jet (Compton and Johnston (1992), Milanovic and M. Q. Zaman (2004)) is also found to have an effect on the control efficiency (Godard and Stanislas (2006)). Other parameters may include spacing between the jets and the distance from the mean separation line. This parameter was found to govern the lifetime of the induced vortices and specific ranges of optima can be found in the literature (Cuvier (2012)). Finally, the co- and counter-rotating arrangements may be seen as another parameter. However, there is no general consensus on the arrangement leading to better control efficiency. For two-dimensional flow separation, Lögdberg (2008) and Godard and Stanislas (2006) suggest that the counter-rotating configuration leads to better results.

For energy saving and real-time adaptability prospects, development has been pushed towards pulsed operating VG jets. Periodic vortical structures are indeed generated with a reduction of the mass flow injected compared to a continuous actuation. Globally, for given equivalent blowing conditions, such as wall-normal blowing for example, an increase in efficiency is obtained when pulsed actuation is used (McManus et al (1994), Ortmanns et al (2008)). When active control is considered, pulsed configurations offer a larger variety of input parameters and consequently open the door to more flexible control strategies than those provided by continuous blowing: jet excitation frequency (f), amplitude or baseline jet to flow velocities ratio (VR), duty cycle (DC) and phase between actuators.

To achieve fast response and make separation control effective, considering the steady flow only is not sufficient. The transient dynamics during the reattachment and relaxing processes must indeed be characterized. Several investigations into the transient regimes of two-dimensional separated flows have been reported in the past (Amitay and Glezer (2002), Darabi and Wygnanski (2004), Mathis et al (2009), Woo et al (2009), Kerstens et al (2011), Shaqarin et al (2013)). The reattachment dynamics can be quantified by a characteristic rising time τ_r. This time is usually scaled into a reduced time scale: $\tau_r^+ = \tau_r\ U_0\ /\ L_{sep}$. The time response of the transient reattachment and relaxation regimes are found to be substantially larger than the actuation time scale (Mathis et al (2009), Shaqarin et al (2013)). This allows in closed-loop control to react rapidly to changes of the flow state. The effect of the actuation frequency of synthetic jets on the reattachment dynamics was examined by Darabi and Wygnanski (2004). An optimal reduced frequency $F_{opt}^+ = f_{opt}\ L_{sep}\ /\ U_0 \approx 1.5$ leading to a minimal reattachment time ($\tau_r^+ \approx 16$) was found for different adverse pressure gradient strengths (varied through changes of geometry) and different amounts of momentum injected in the flow. During the transition, a slow flapping motion was observed in the shear layer region.

Instantaneous survey of the wall friction using friction probes such as hot-film sensors has been shown by some authors to offer the potential, first, to give a measure of the reattachment state once calibration is effected or once friction level over which the flow is reattached is properly known (Stalnov et al (2007), Mathis et al (2009), Chabert et al (2013), Shaqarin et al (2013)), and secondly, to be a reliable flow metric for closed-loop control (Nakayama et al (1993)).

From the previous works on transient reattachment (Amitay and Glezer (2002),Darabi and Wygnanski (2004), Mathis et al (2009), Siauw (2008)), only the separation region or the wake have been studied without simultaneous characterization of the incoming boundary layer. The convection of flow coming from the actuators is not observed in the flow fields for example. Furthermore, the transient characterization is usually reduced to one characteristic reattachment time, whereas different characteristic times can be determined considering different measurements techniques and different positions in the flow field. The objective of the present study is to realize simultaneous measurements of the friction gain at the wall and the phase-averaged velocity to fully characterize the reattachment and to determine characteristic times of this phenomenon from different sensors. The experimental set-up is described in section 2. The separating boundary layer considered as the baseline flow is presented in section 3 and the separation bubble characteristics, particularly its length and area, are provided. The effect of pulsed actuation on the friction gain measured by hot-film sensors is then considered in section 4. Characteristic times τ_r of the reattachment are obtained from these measurements for continuous and pulsed actuation by fitting a first-order model on the friction gain dynamics. The phase-averaged velocity field is eventually investigated in section 5 using the phase-locked mean velocity and turbulent kinetic energy. The controlled flow under pulsed action is first considered (§ 5.1), then the transition between separated and reattached flows (§ 5.2) is assessed. The separation bubble dynamics is quantified through integral quantities (§ 5.3) and, finally, the dynamics of the complete flow is studied with conditional Proper Orthogonal Decomposition (§ 5.4). The aim is to understand the dynamics of reattachment and to compare the characteristic times from the phase-averaged velocity with those determined from the friction signals.

2 Experimental facilities

2.1 Flow and ramp model

The experiments are conducted in the closed loop boundary layer wind-tunnel at Laboratoire de Mécanique de Lille. The wind tunnel includes a 20 m long test section with a constant cross section of 2m$\times$1m along which the boundary layer develops. The maximum freestream velocity and turbulence level are 10 m/s and 0.3% respectively. Under operation, the temperature is regulated to ±0.2°. Full details on the wind tunnel and its characterization can be found in Carlier and Stanislas (2005).

Beyond 14.4 m from the beginning of the test section, the boundary layer encounters a two-dimensional ramp. The ramp model is shown in figure 1. It is constituted of four parts: **(i)** a smooth converging part with a contraction ratio of 0.75, **(ii)** an articulated flat plate 2.14 m in length with an angle of -2° relative to the floor of the wind-tunnel, **(iii)** an articulated flap 0.34 m long with an angle of $-22°$, and finally **(iv)** a flexible plastic sheet ensuring smooth connection to the floor of the wind tunnel. In the following, the leading edge of the flap is used as origin of coordinates. The height of the ramp H_s at the leading edge is 17.5 cm. At $U_\infty = 10$ m/s, the boundary layer thickness just before separation is $\delta = 0.19$ m and the reference streamwise freestream velocity at this position is $U_0 = 12.3$ m/s. A complete characterization of the flow along the ramp upstream of the separation line can be found in Cuvier et al (2014). The flow is essentially two-dimensional over 70% of the flap span, except near the side walls where side wall effects are observed. Measurements are realized at the wind tunnel middle where the flow can be considered 2D.

2.2 Flow control actuators

A spanwise array of 22 co-rotating round jets of $\phi = 6$ mm in diameter located 1.3δ upstream of the separation line is used for actuation. To generate continuous or pulsed actuation, the apparatus proposed

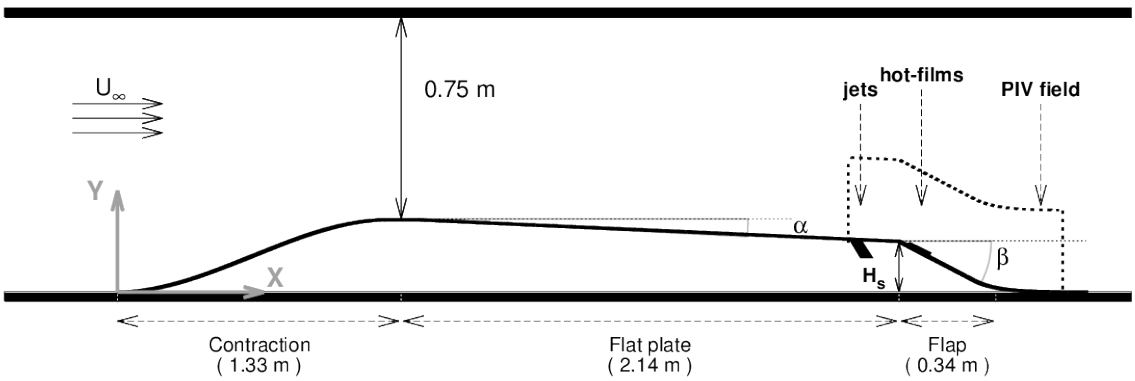

Fig. 1 Schematics of the experimental set-up and main dimensions of the ramp geometry.

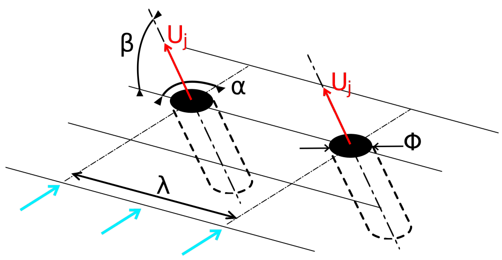

Fig. 2 Co-rotating configuration of the actuators used in this study. $\phi = 0.03\ \delta$ is the diameter, $\alpha = 125°$ the skew angle, $\beta = 35°$ the pitch angle, $\lambda = 13.6\ \phi$ the spacing between two jets.

by Braud and Dyment (2012) and further implemented and characterized by Shaqarin et al (2013) is used. Air is supplied to Festo valves by a 75 kW compressor through a first tank of 2 m^3 and a secondary 0.09 m^3 reservoir which allows damping of pressure variations. The flow rate is fixed by sonic throats, 1.3 mm^2 in cross section, located just downstream of the valves. Figure 2 shows the jets configuration considered in the present work: the jets are blowing in the upstream direction with a skew angle of $\alpha = 125°$, and a pitch angle $\beta = 35°$. The spacing between two consecutive jets is $\lambda = 0.43\ \delta$ and the exit jet diameter is $\phi = 0.03\ \delta$. Uniformity of the actuation in the spanwise direction, essentially sensitive to the throat diameters, has been checked without the incoming flow and an average dispersion of 4.8% of the outlet velocity, measured with a Pitot tube, was observed over the 22 valves. The temperature at the jet exit was also measured and a difference smaller than 1.2°C was recorded whatever the control input parameters are.

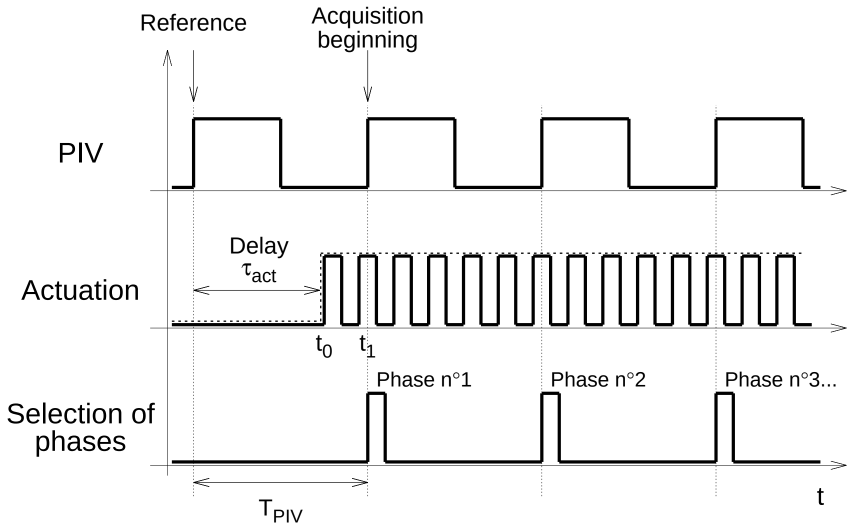

Fig. 3 Illustration of signal synchronization with (a) PIV reference signal, (b) actuation input and (c) selected PIV phases.

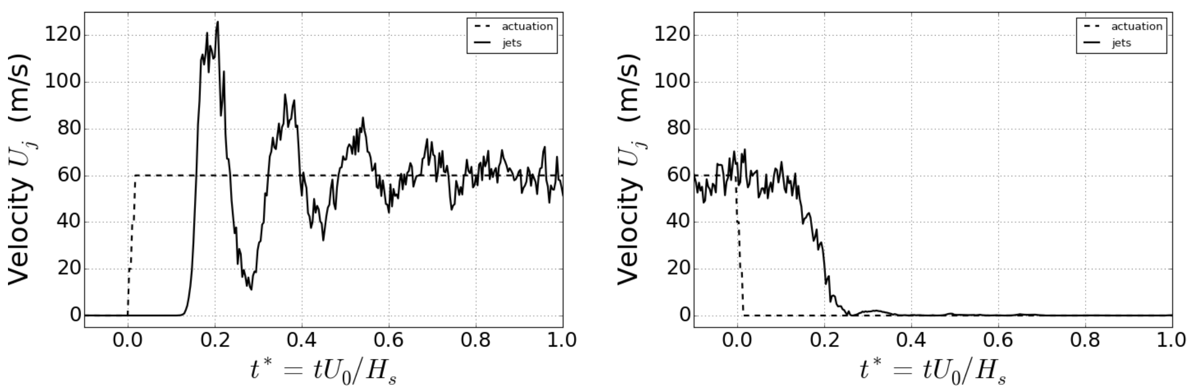

Fig. 4 Time response of the actuator's exit velocity during (a) activation and (b) desactivation of the valves for continuous blowing.

The valves are driven by an Arduino micro-controller which allows to generate continuous or pulsed actuation. The Arduino board has an internal clock frequency of 16 MHz which enables input signal to be generated with a time precision of 125 ns. Since analysis of the transient dynamics during separation and reattachment regimes are here of particular concern, cycles of forcing/unforcing flow regimes are repeated. These cycles are divided into 5 s of forcing for flow reattachment (jets actuation turned on) and 5 s during which the flow is unforced and recovers a separated state (jets actuation turned off). The duration of 5 s was chosen based on the results of Shaqarin et al (2013) and allows the flow to reach steady attached or separated states. An illustration of the command signal sent to the valves is shown in figure 3. During the forcing period, pulsed signals are generated with given frequency f and duty cycle DC such that the valves are successively opened for a duration $DC\ /\ f$ and closed during $(1 - DC)\ /\ f$. In order to fully investigate the receptivity of the flow, and to model the flow response to a given actuation in perspective of closed-loop control, the range of control parameters also includes the velocity ratio $VR = U_j\ /\ U_\infty$ defined as the ratio between the jets exit velocity and the baseline freestream velocity above the actuators. The dimensionless mass flow coefficient $< c_\mu >$ used to quantify the average mass flow rate injected and representative of the energy cost is expressed on one actuation period T:

$$< c_\mu >= DC\ \left(N_j\ \rho_j\ U_j^2\ S_j\right)\ /\ \left(0.5\ \rho_0\ U_0^2\ \delta\ \lambda\right) \tag{1}$$

where N_j is the number of actuators, ρ_j and ρ_0 the air density at the jets exit and of the free stream respectively, and S_j the jet exit area. The frequency of actuation is also given as a non-dimensional reduced frequency expressed as $F^+ = f\ L_{\text{sep}}\ /\ U_\infty$ where $L_{\text{sep}} = 0.59$ m is the separation bubble length for the baseline flow.

Before turning to flow control experiments, the actuators were fully characterized in terms of jet speed with regards to the different control parameters invoked previously. It is in fact crucial to ensure that the actuators provide the required velocity (static characterization) and respond much faster than the characteristic times of attachment and separation (dynamic characterization). Figure 4 shows a typical time history of the jet exit velocity measured with a hot-wire located at the jet exit. Results for continuous blowing jets are considered. An overshoot of the jet exit velocity at the valve opening and oscillations are first observed. These oscillations have already been observed by Kostas et al (2007) and explained by Braud and Dyment (2012). They are the consequences of an acoustic shock wave created by the sudden pressure increase: the shock wave travels between the sonic throat output and the tube output, where it reflects back toward the sonic throat and realizes several round trips before disappearing by viscous dissipation. An overshoot of the static velocity value happens 3 ms after the valve opening, which is negligible compared to the convection time needed for a vortical structure to travel from the actuator to the hot-film sensor (approximately 55 ms at $U_\infty = 10$ m/s) as discussed later. This value of 3 ms is also comparable with the response time of solenoid valve used by Siauw (2008), for example, for separation control over an airfoil. The same trend and same characteristic time response is observed when the actuation is turned off as illustrated in figure 4(b).

2.3 Metrology

The flow dynamics in the separated region and along the wall during the transients is investigated here for both separation and reattachment. For this purpose, simultaneous measurements using phase-locked PIV and hot-film sensors were performed.

For the flow field study, two-dimensional two-component (2D2C) phase-locked PIV measurements were performed in a streamwise/wall-normal plane as illustrated in figure 5. The measurement plane was located at the wind-tunnel mid span ($z = 0$), midway between two consecutive jets. Four Hamamatsu cameras with a resolution of 2048×2048 px^2 each were used to cover the entire region of interest. This includes the region upstream of the flap where the incoming boundary layer is not yet separated, the flap with the separation bubble and the reattachment region downstream the geometry. The overall field of view is 5δ long and 1.5δ high. This optical arrangement is fully detailed in Cuvier (2012). To obtain correct matching of the final vector fields, the four fields of view obtained from each camera were overlapped and the meshing procedure developed by Cuvier (2012) was used. The laser sheet was provided by a Nd-Yag Laser with an energy of 400 mJ per pulse. PIV images were acquired at 4 Hz and processed with an in-house software (adapted from the MatPIV 1.6.1 toolbox written by J.K. Sveen) using standard multi-grid/multi-pass cross-correlations approach with a final spatial resolution of 1.5 $\times$ 1.5 mm^2. The merging regions were used to estimate the measurement uncertainty as described by Foucaut et al (2014). Maximal random errors of 0.25 px far from the wall and 0.7 px near the wall were obtained. The error decreases along the ramp.

To capture the transient dynamics during flow reattachment and separation despite the limitation of the PIV system with regards to the low repetition rate, a phase-locked procedure was used. During the blowing period, a limited number of points in time are considered as phases, hereafter denoted $\{t_k\}$ with $k = 1, ..., N_p$. Phases of the transient regimes are here arbitrarily selected and PIV fields corresponding to these phases are collected and averaged. Given $\mathbf{u}(\mathbf{x}, t)$ the instantaneous velocity, the phase-averaged velocity can be expressed as:

$$\widehat{\mathbf{U}}(\mathbf{x}, t_k) = \frac{1}{N_c} \sum_{n=0}^{N_c-1} \mathbf{u}(\mathbf{x}, t_k + nT_c) \quad k = 1, ..., N_p \tag{2}$$

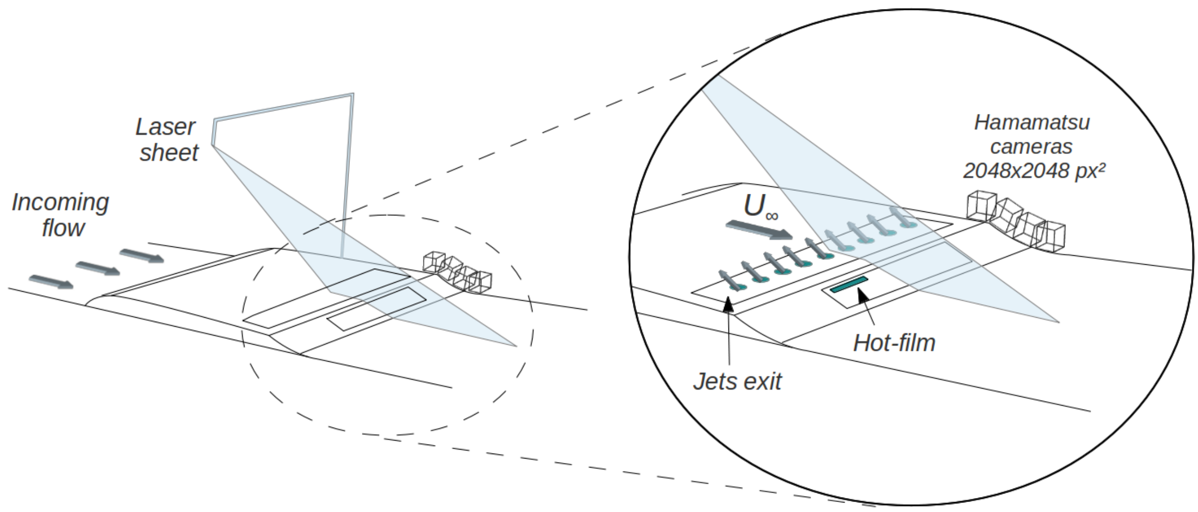

Fig. 5 Schematics of the 2D2C PIV set-up.

where N_c is the number of repeated cycles of actuation of duration T_c (here T_c =10 s). This procedure is obtained by synchronizing the actuation signal with the PIV clock as reference signal. The synchronization procedure is schematically illustrated in figure 3. Due to the limitation of the PIV rate at 4Hz, experiments were repeated and conducted by modifying the value of the time-delay τ_{act} used to start the acquisition of the PIV snapshots with regards to that of the cycles raising edges (see figure 3). Following this procedure, a phase-averaged flow field sampled at 64Hz was obtained and will be used to characterize the flow transients during reattachment. A number of $N_c = 500$ was found sufficient to ensure statistical convergence. In the present case, using this method, 16 different experiments at acquisition frequency of 4 Hz were performed to obtain phase-average fields at a resolution of 64 Hz.

The survey of the skin friction in the separation region is provided by an array of hot-film sensors (Senflex SF9902), located on the flap. The position of each sensor of the array is given in table 1. The sensitive part is 1.5 mm long and 0.1 mm wide. It is deposited on a polyamide substrate with a thickness less than 0.2 mm. All the sensors are connected to an AN1003 constant anemometer manufactured by AAlab Systems. The pseudo calibration procedure detailed in Godard & Stanislas (2006) is applied such that the output voltage can be considered as representative of the skin friction along the wall with enough repeatability and accuracy. For the present experiments, hot-film signals were sampled at 10 kHz to fulfill the Shannon's sampling criteria. In the following, the phase-averaged response of these signals to repeated cycles of actuation, noted $E(t) - E_0$, is computed, with E_0 the hot-film signal obtained for the separated flow, in a way similar to the phase-averaged velocity in equation 2. For the next sections, the freestream velocity is fixed at $U_\infty = 10$ m/s. Two actuation cases are considered at a velocity ratio $VR = 5$: continuous and pulsed actuation (duty cycle $DC = 50\%$, frequency $F^+ = 0.38$).

3 Separated flow without control

Before describing the effect of the actuation, the overall baseline separated flow is characterized. Figure 6 presents (a) the streamwise mean velocity U_{mean} and (b) the Turbulent Kinetic Energy (TKE) $k = \frac{1}{2}\left(u'^2 + v'^2\right)$ scaled by the reference streamwise velocity U_0 at the leading edge far from the wall ($U_0 =$ 12.3 m/s). The location of the recirculation region is highlighted by the separation line using the backflow coefficient χ (Simpson (1989)) with a value of 0.5.

Sensors		X/H_s	Z/H_s
Streamwise location	SX_1	0.49	-0.46
	SX_2	0.66	
	SX_3	0.94	
	SX_4	1.29	
Spanwise location	SZ_1	0.49	-0.46
	SZ_2		-0.35
	SZ_3		-0.23
	SZ_4		-0.12
	SZ_5		0.12
	SZ_6		0.23
	SZ_7		0.35
	SZ_8		0.69

Table 1 Spatial position of the hot-film sensors used to characterize the transient dynamics of friction gain on the flap.

Using this criterion, the separation point is located $0.1H_s$ downstream of the leading edge of the flap while the separation length is estimated as $3.4H_s$. The region between the freestream and the recirculation area is dominated by high velocity gradients and a high level of turbulent kinetic energy as shown in figure 6(b). The streamwise component of the velocity fluctuations is nearly 90% of the peak of TKE and dominates near the separation point. This is mostly due to the Kelvin Helmholtz instability developing from the separation point. Linked to the flapping mode of the separation bubble, the wall-normal component dominates near the reattachment point and downstream of it.

4 Transient dynamics of friction gain

The effect of the actuation on the separated flow is now considered. Phase-averaged response of the friction gain located at $X\ /\ H_s = 0.49$ along the flap is reported in figure 7. The friction gain signal

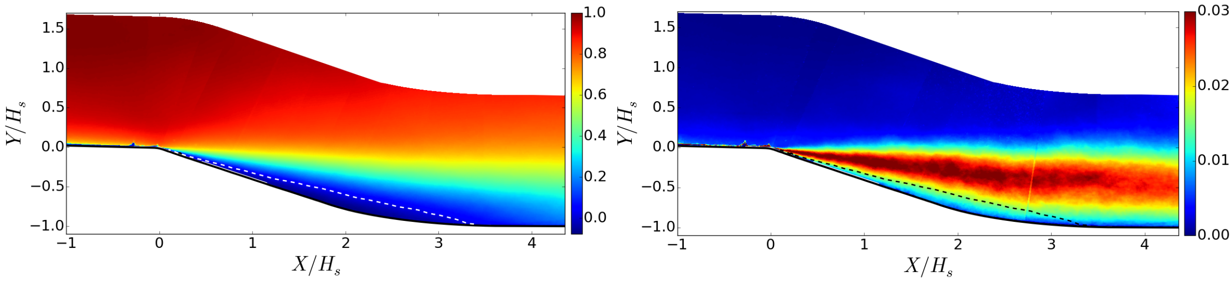

(a) $U_{mean}\ /\ U_0$ (b) $\frac{1}{2}\left(u'^2 + v'^2\right)\ /\ U_0^2$

Fig. 6 Evolution of (a) the average streamwise velocity field $U_{mean}\ /\ U_0$ and (b) the turbulent kinetic energy $k\ /\ U_0^2 = \frac{1}{2}\left(u'^2 + v'^2\right)\ /\ U_0^2$ of the separated flow. The thick continuous line corresponds to the wall, the dotted line to the mean separation line detected by the χ criterion.

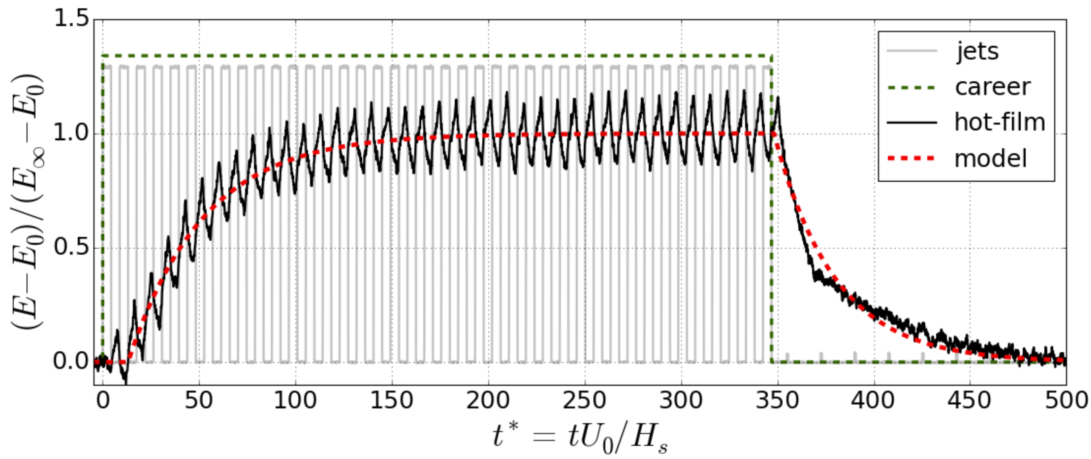

Fig. 7 Friction gain response $(E(t)-E_0)/(E_\infty-E_0)$ to pulsed actuation for hot-film sensor SX_1 located at $X\ /\ H_s = 0.49$ from the leading edge of the flap. green dotted line: actuation career window, gray line: actuation signal, black line: friction gain, red dotted line: first-order model fitted on the friction gain response.

$E(t) - E_0$ is scaled by the steady friction gain $E_\infty - E_0$ for the controlled flow. The continuous black line shows the hot-film response to the jets actuation driven by the excitation signal shown in continuous gray line. Regimes corresponding respectively to uncontrolled and controlled flows are manifest. When the actuation is turned on, at $t^* = 0$, the friction gain first increases suggesting flow attachment, before reaching a stationary controlled regime above $t^* \simeq 200$. During this regime, the fairly periodic oscillations observed correspond to the signature of convected vortical structures generated by the actuators and interacting with the boundary layer. The frequency of these oscillations is directly related to the frequency of actuation while their amplitude also depends on the velocity ratio. When the actuation is turned off ($t^* = 350$), the friction gain shows a rapid decrease towards the reference value achieved when the flow is fully separated (for $t^* < 0$), indicating that the flow returns to the state before actuation. It is noteworthy that the reattachment and separation processes observed here happen with a time delay between the actuation and the hot-film response. This time shift is mostly due to the convection time of the structures generated by the actuators and is estimated to be about 55 ms ($\simeq 3.9 H_s/U_0$) for SX_1.

As suggested by Shaqarin (2011) and as reported in figure 7, the tendency of transients towards the separation and reattachment regimes can both be modeled as first-order response. This allows characteristic time for reattachment $\tau_r^+ = \tau_r \ U_0 \ / \ L_{sep}$ and separation $\tau_s^+ = \tau_s \ U_0 \ / \ L_{sep}$ to be estimated. Characteristic times of $\tau_r^+ = 11.7$ and $\tau_s^+ = 9.4$ were found respectively in the present study. The different model parameters were estimated for each set of actuation parameters in Raibaudo (2015).

The information contained in the friction gain as discussed above gives only a local view of the flow response. Hot-film sensors distributed at various streamwise and spanwise locations have therefore been used to allow a better understanding of the flow response over the flap. The transient response of hot-film sensors distributed along the streamwise direction at $Z \ / \ H_s = -0.46$ and the corresponding characteristic time τ_r^+ are reported in figure 8. Four streamwise positions SX_i of sensors are considered (table 1). The stabilized friction signal is found to decrease with the streamwise distance X/H_s. A consequence of this is the increase of the reattachment time as moving away from the leading edge. This is illustrated in figure 8(b) where $\tau_r^+ = \tau_r \ U_0 \ / \ L_{sep}$ is reported as a function of X/H_s. Tilmann et al (2006) suggest that this is due to the fact that the structures generated by the jets loose their strength rapidly when convecting downstream and move away from the wall.

Similarly, the evolution of the steady friction gain and characteristic time are considered in figure 9 along the spanwise direction at $X \ / \ H_s = 0.49$. For each sensor SZ_i, the steady friction gain $(E_\infty - E_0)_i$ is scaled by the averaged steady gain along the span $\overline{E_\infty - E_0} = \sum_{SZ_i} (E_\infty - E_0)_i$. The location of the actuators with respect to the hot-film sensors, as well as the direction of the co-rotating structures generated by the jets are also indicated. The friction gain is found to vary significantly in the spanwise

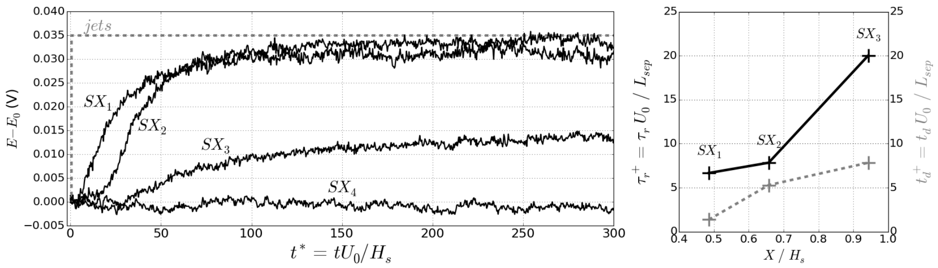

Fig. 8 Streamwise distribution of the friction gain $E - E_0$ (in volts) during the reattachment **(a)** and corresponding rising time $\tau_r^+ = \tau_r \ U_0 \ / \ L_{sep}$ (black) and delay $t_d^+ = t_d \ U_0 \ / \ L_{sep}$ (grey) function of the streamwise sensor position X/H_s **(b)**. A continuous actuation at $VR = 5$ for $U_\infty = 10$ m/s is considered for this figure.

direction. Large values of friction gain are observed for sensors located below the expected vortical structures while sensors aligned with the actuators exhibits lower values. The reattachment time τ_r^+ behaves in an opposite way: sensors located below vortical structures exhibit low rising time (which means fast response). As observed also by Kostas et al (2007) using PIV in a spanwise/wall-normal plane, this confirms the three-dimensionality of the structures generated by the pulsed jets and hence of the controlled flow.

5 Description of flow transients under control

Modeling the hot-film response in the perspective of implementing closed-loop controllers is not sufficient. Identifying the state and the characteristic time scales of the flow itself when actuated is of crucial importance too. In this section focus is put on the flow transients thanks to the phase-locked PIV data sequences obtained. Phase-averaged mean velocity components and phase-averaged kinetic energy are evaluated according to equation 2.

5.1 Dynamics of the stationary controlled state

The phase-averaged streamwise velocity and turbulent kinetic energy during a period of control is presented in figure 10. During the stationary regime, as already discussed in section 4, the friction signal exhibits periodic oscillations and is shown in the lower left corner of each sub-figure. The first and last

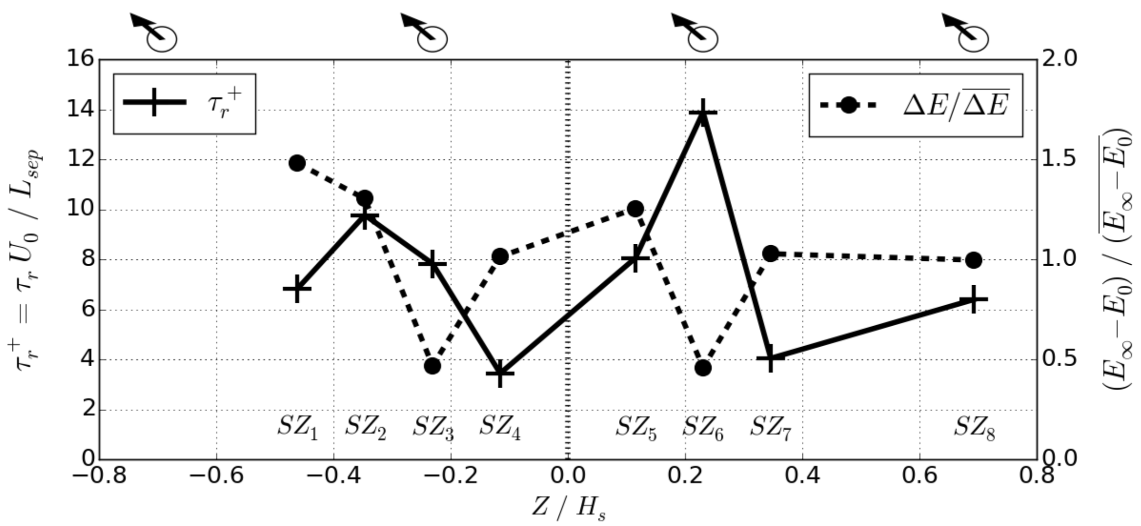

Fig. 9 Spanwise distribution of (•) steady friction gain $(E_\infty - E_0)/(\overline{E_\infty - E_0})$ and (+) reattachment time τ_r^+. A continuous actuation at $VR = 5$ for $U_\infty = 10$ m/s is considered for this figure. The spanwise locations of the actuators are indicated by (∘) while the black arrows gives the expected direction of the actuation flow generated by the jets. The jets are located at 2.10 H_s upstream the hot-films sensors line.

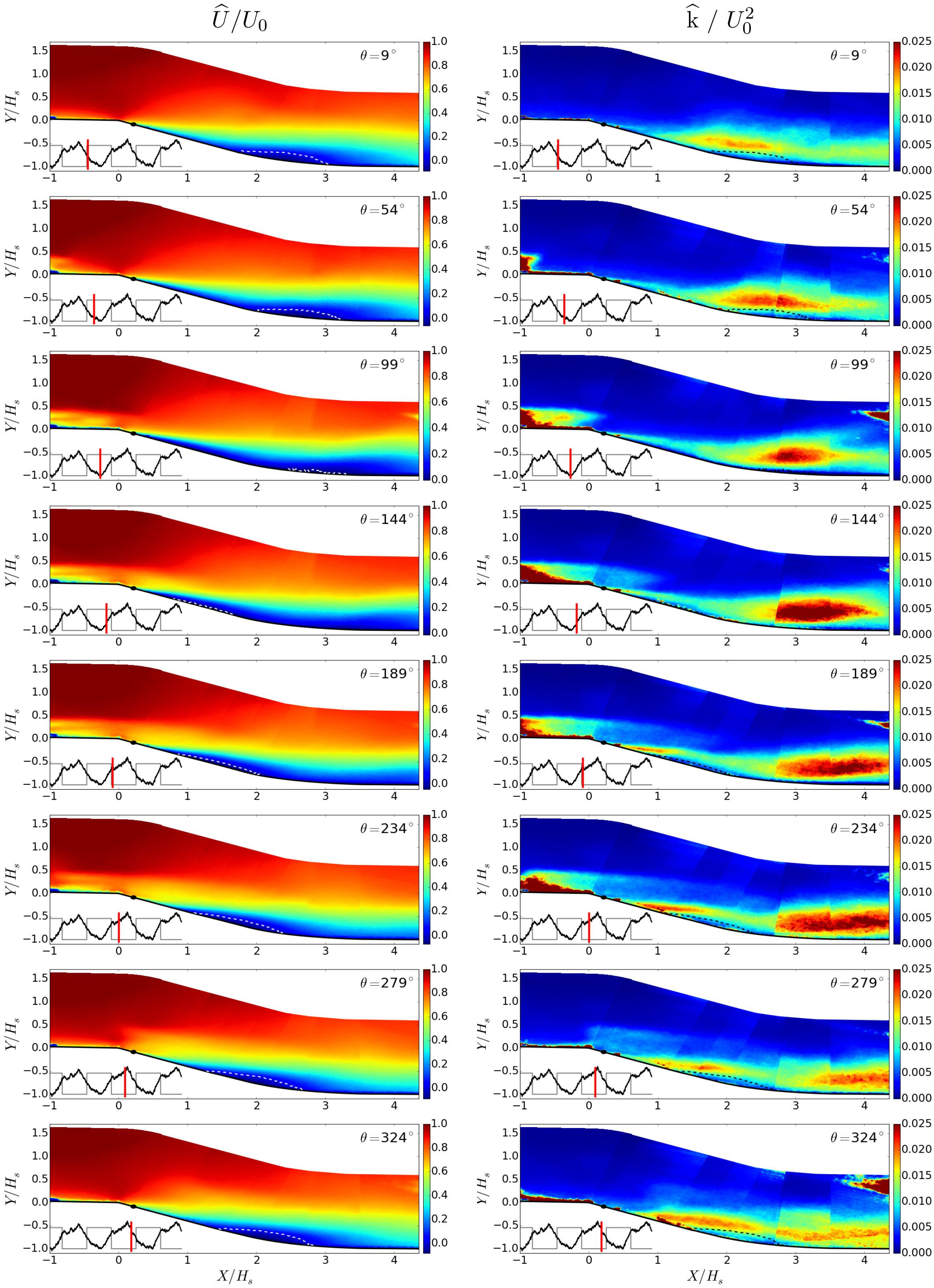

Fig. 10 Evolution of the phase-averaged (first column) streamwise velocity $\widehat{U}/U_0$ and (second column) the turbulent kinetic energy $\widehat{\mathrm{k}}\ /\ U_0^2 = \frac{1}{2}\left(u'^2 + v'^2\right)/U_0^2$ for a stabilized flow with pulsed actuation ($U_\infty = 10$ m/s, $VR = 5$, $F^+ = 0.38$, $DC = 50$ %, $< c_\mu >= 4.1 \times 10^{-2}$). The phase in degrees is $\theta = (t^\star/T) \times 360°$ and $t^\star$ the temporal position in the period T ($0 \leqslant t^\star < T$). The thick continuous line corresponds to the wall, the dotted line to the mean separation line detected by the χ criterion.

snapshots in figure 10(a), which are separated by 315° of phase, are quite similar which confirms that a stationary regime is reached. Consequently, the flow dynamics is considered independent of the actuation origin and the phase instant is expressed as $\theta = (t^\star/T) \times 360°$, with $t^\star$ the temporal position in one period T $(0 \leqslant t^\star < T)$.

During an actuation period, the separation bubble is pushed downstream, reducing in size and totally vanishing at $\theta = 99°$, before reappearing at the top of the flap. Compared to the baseline (fig. 6), the regenerated bubble is shorter in length ($L_{sep} = 1.4H_s$ for $\theta = 279°$). An increase of the level of fluctuating energy above the separation bubble is also observed in figure 10(b). Pockets of turbulence are periodically generated on the flap and convected downstream. In the present conditions, the periodic actuation is unable to fully reattach the flow. It maintains an unsteady partial reattachment, with strong fluctuations along the flap.

5.2 Dynamics of the attachment

The phase-averaged flow response during the reattachment process, once the actuation is activated, is illustrated in figure 11 and 12 where the phase-averaged streamwise velocity and the phase-averaged kinetic energy are reported respectively at a selection of given phases $t_i^* = t_i U_0/H_s$ (with $t_i = t_1 + (i-1).f_{PIV}$ the phase instants, $t_1 = 3.125$ ms the first phase instant and $f_{PIV} = 64$ Hz the phase sampling frequency). The corresponding hot-film response (whose spatial location on the flap is highlighted by the black circle) is also given at the bottom left of each subfigure.

The sequences do not show any modification of the separation area until $t^* = 3.5$, also visible in the friction signal evolution. This time corresponds to the delay needed by the vortical structures to convect to the separation region. The convection of the structures is visible in the velocity map. In contrast to a large number of studies reported in the literature, the perturbation introduced by the actuators remains here limited to the boundary layer region. A third of the boundary layer thickness is affected when the jets are activated ($y_{perturb}$ / $\delta_0 = 0.36$). For the chosen F^+, the actuators are turned off at $t^* = 4.4$ and reactivated at $t^* = 8.8$. Due to convection, the new vortical structures reaches the leading edge of the flap at $t^* = 12.3$. In the transient phase, the separation point is first pushed downstream while the reattachment point is not affected. The separation bubble inflates, increases in height, then moves downstream while its area drastically decreases. The formation of a new separation starting at the leading edge is visible from $t^* = 11.2$. The new bubble is smaller in size compared to the baseline one. The turbulent kinetic energy in figure 12 shows a strong reduction reaching 23% after one pulse at $t^* = 9.0$. After $t^* = 9.0$, the turbulent region strongly inflates while being pushed downstream and growing in intensity. Production of high level of TKE is observed at the leading edge, announcing the formation of a new shear layer and separation.

In conclusion, about two trains of vortical structures (corresponding to two pulses of actuation) are necessary to drive the flow to a stationary new state. The velocity field responds apparently faster to the actuation compared to the hot-film sensors.

5.3 Dynamic behavior of integral quantities

In the previous sections, a description of the transients have been reported showing how the flow qualitatively responds to pulsed actuation. The response in terms of separation length and separation area are now described. The separation length is defined using the separation bubble detected by the χ criteria:

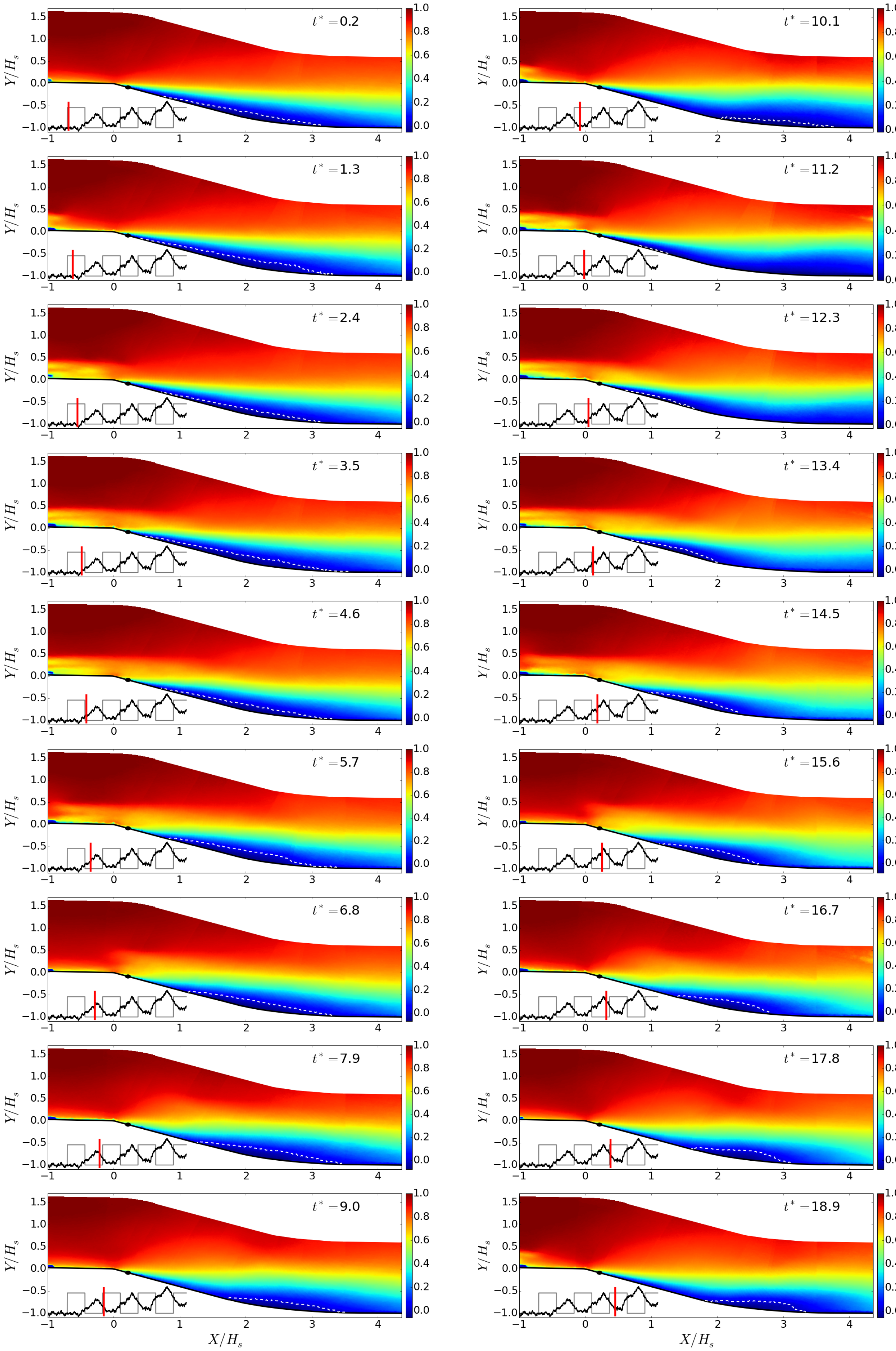

Fig. 11 Evolution of the phase-averaged streamwise velocity $\widehat{U}/U_0$ for a stabilized flow with pulsed actuation ($U_\infty = 10$ m/s, $VR = 5$, $F^+ = 0.38$, $DC = 50$ %, $< c_\mu >= 4.1 \times 10^{-2}$) for each phase instant $t_i^* = t_i U_0/H_s$. The thick continuous line corresponds to the wall, the dotted line to the mean separation line detected by the χ criteria.

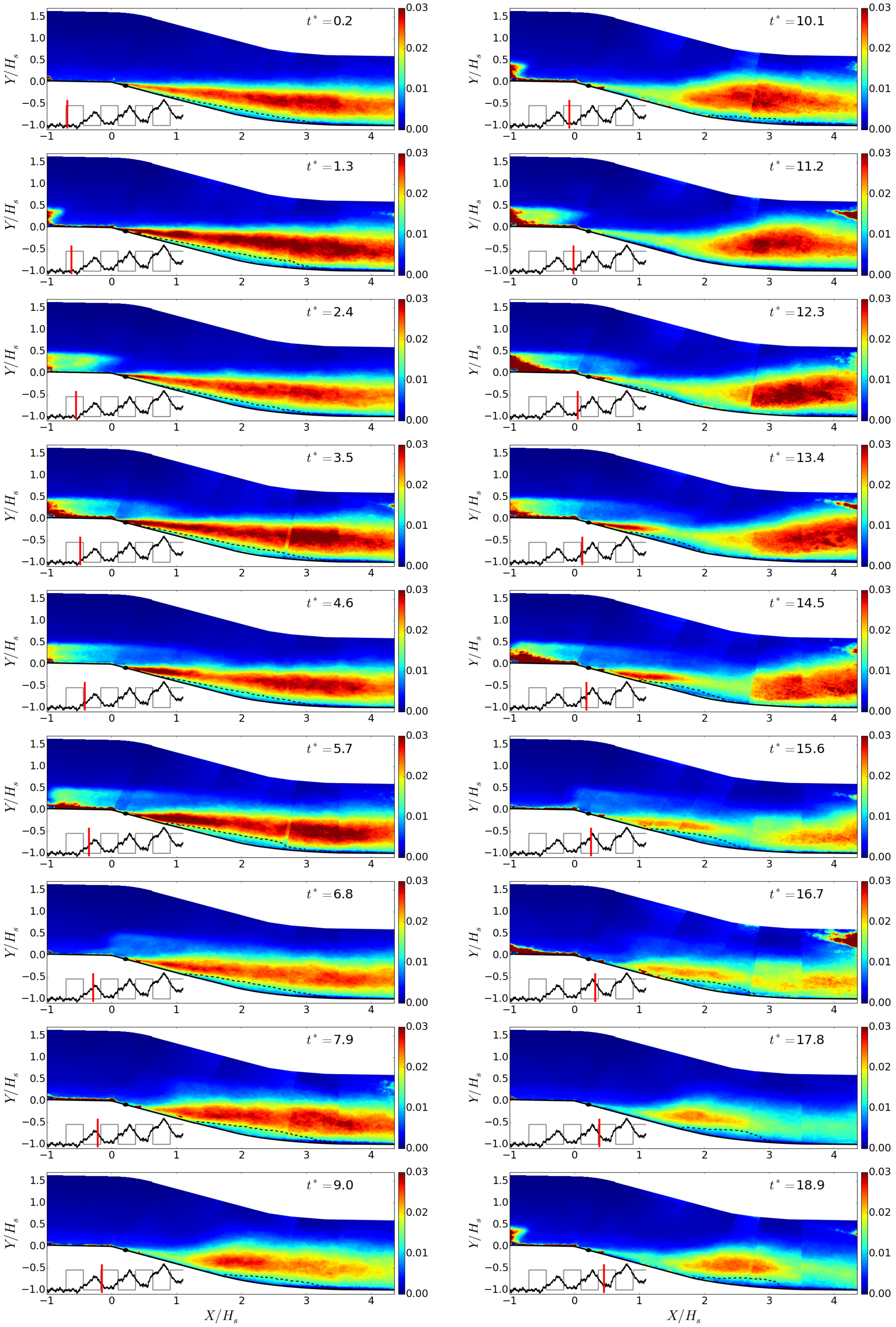

Fig. 12 Evolution of the total turbulent kinetic energy $\widehat{\mathrm{k}}$ / $U_0^2 = \frac{1}{2}\left(u'^2 + v'^2\right)$ / U_0^2 for a stabilized flow with pulsed actuation ($U_\infty = 10$ m/s, $VR = 5$, $F^+ = 0.38$, $DC = 50$ %, $< c_\mu >= 4.1 \times 10^{-2}$) for each phase instant $t_i^* = t_i U_0 / H_s$. The thick continuous line corresponds to the wall, the dotted line to the mean separation line detected by the χ criteria.

$$L_{sep} = \int_{L_{PIV}} \delta^H(s) \ \ ds \quad \text{ with } \ \delta^H(s) = \begin{cases} 0 & if \ H_{sep}(s) < \epsilon_H \\ 1 & \text{otherwise} \end{cases} \tag{3}$$

with s the curvilinear coordinate along the entire PIV domain of streamwise length L_{PIV}, H_{sep} the separation bubble height and $\epsilon_H = 0.5\%$ $H_{sep,max}$ a threshold depending of the maximal separation height $H_{sep,max}$ detected. This separation length has been often used in literature as a control objective (Simpson (1989), Chun and Sung (1996), Hasan (1992), Gautier and Aider (2014)). Time history of $L_{sep}(t)/L_{sep,0}$ under flow actuation is reported in figure 13(a) ($L_{sep,0}$ is the separation length without actuation). For $t^* > 11.2$, the separation length evolution is almost periodic and stabilized. The skewness of the signal in the stationary regime is clear and indicates that the length of the separation bubble does not change significantly while being pushed downstream as was already observed in §5.1. The plateau indicates that most of the time $L_{sep} \approx 0.55 L_{sep,0}$. The fact that $L_{sep} = 0$ is never reached indicates that there is on average always a separation in the field of view, although not at the same location.

The second quantity examined here is the separation area defined as,

$$A_{sep} = \int_{L_{PIV}} H_{sep}(s) \ \ ds \tag{4}$$

where H_{sep} is the separation height. Time history of $A_{sep}(t)/A_{sep,0}$ (where $A_{sep,0}$ is the area of the separation bubble of the baseline flow) is reported in figure 13(b). In contrast to the separation length, large amplitude variations of the separation area are observed during the stationary regime with almost periodic oscillations going nearly down to zero and an almost zero skewness. While being pushed downstream, the bubble height is significantly reduced in contrast to the separation length which remains

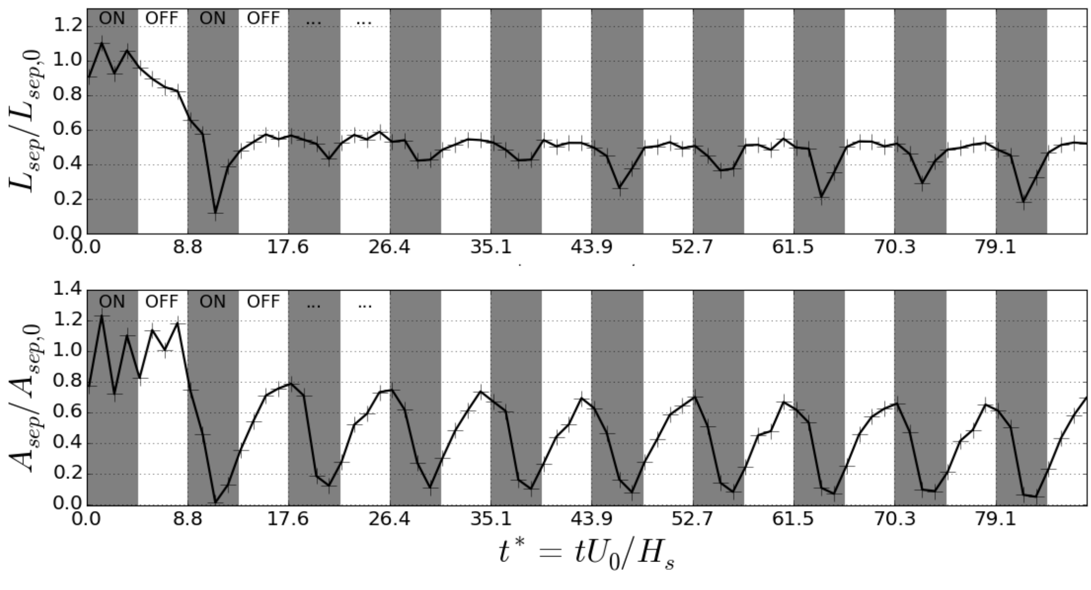

Fig. 13 Evolution in time of the (a) the separation length and (b) the separation area for pulsed case ($U_\infty = 10$ m/s, $VR = 5$, $F^+ = 0.38$, $DC = 50$ %, $< c_\mu >= 4.1 \times 10^{-2}$). In grey the actuation periods.

almost constant. Minima of separation length and area coincide, corresponding to the bubble disappearance downstream. During the transient, the separation length starts to decrease around $t^* = 3.5$, while the separation area reacts only for $t^* > 7.9$. This was already observed in figure 11, the separation bubble moves downstream with an increase in height and a reduction of length, resulting in a nearly constant area and position of the reattachment point. It is interesting to note that the first pulse removes almost completely the separation length and area. The characteristic rising time is $\tau_r^+ = 4.8$ for the separation length, which is lower than for the friction signal. No first-order model can be fitted on the separation area response.

5.4 Analysis of the dynamic behavior using Conditional Proper Orthogonal Decomposition

To try to characterize the transient dynamics of the attachment using the complete velocity field and not only integral quantities of the separation bubble, an approach based on Proper Orthogonal Decomposition was used. The interest of this technique is to allow the construction of temporal modes based on the whole velocity field representative of the unsteady behavior of the controlled flow. As shown in figure 14, to focus on the separation region, only the phase-averaged streamwise velocity $\widehat{\mathbf{U}}_{\mathbf{b}}(\mathbf{x}, t_p) = \widehat{\mathbf{U}}(\mathbf{x}(X > 0, Y), t_p)$ starting at the leading edge is considered. The Conditional Proper Orthogonal Decomposition (CPOD) procedure, developed by Siauw (2008), is applied here using the evolution in time of the phase-averaged velocity as snapshots for the CPOD:

$$\widehat{\mathbf{U}}_{\mathbf{b}}(\mathbf{x}, t_p) = \widehat{\mathbf{U}}_{\mathbf{b}}(\mathbf{x}, t_1) + \sum_{i=0}^{N_m - 1} a_i(t_p)\ \widehat{\mathbf{\Phi}}_i(\mathbf{x}) \tag{5}$$

The first temporal mode a_0 is presented in figure 15. This first mode corresponds to 52 % of the cumulative energy, which is important as expected from a decomposition using phase-averaged velocity. Similarly to the friction gain response, a first-order model with delay can be fitted on this mode using a least-squares method. The rising time obtained is $\tau_r^+ = \tau_r U_0 / L_{sep} = 4.1$. It is lower than the one determined from the friction gain ($\tau_r^+ = 11.7$, fig. 7) and separation length ($\tau_r^+ = 4.8$, fig. 13). These differences are discussed in the next section.

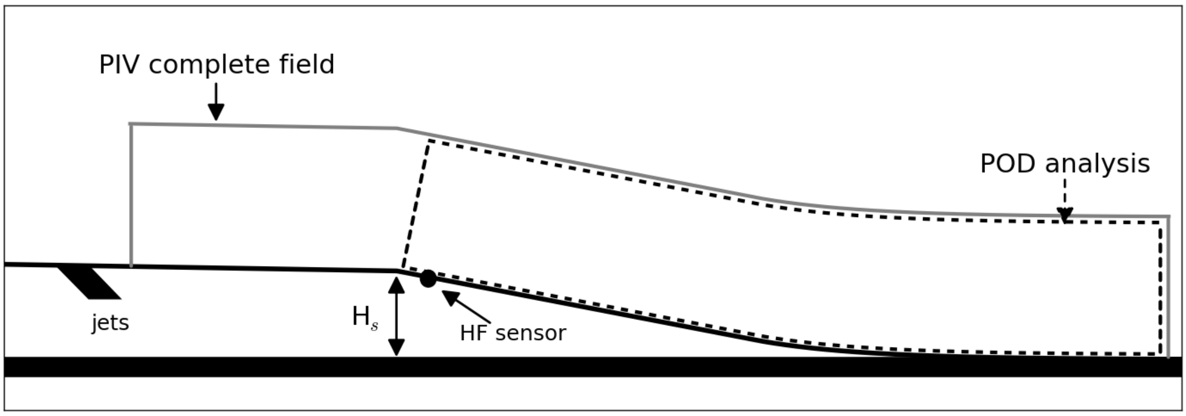

Fig. 14 Spatial range considered for the Conditional Proper Orthogonal Decomposition.

X/H_s	0.49	0.66	0.94	
$X/L_{sep,0}$	0.14	0.19	0.28	
t_d^+	1.4	5.3	7.8	Friction
τ_r^+	6.7 [3. − 14.]	7.8	20.	Friction

Table 2 Comparison of characteristic times obtained from different friction probes at different stations for continuous blowing.

Discussion

Table 2 summarizes the reattachment transient characteristics obtained with the friction probes at the wall in the case of the continuous blowing presented in figure 8. As can be seen from the values of $X/L_{sep,0}$, all probes are initially inside the separation bubble. The PIV data (not shown here, see Raibaudo (2015) p. 280) show that, as for the pulsed actuation case, the separation bubble is first moved toward downstream along the wall before disappearing around $t^+ \simeq 5.0$ and $X/H_s \simeq 3.0$. This explains the downstream evolution of the delay t_d^+ which is correlated with the position of the separation point along the wall and not with a convection of structures by the external velocity. As can be seen from t_d^+, this progression of the separation point is strongly non linear.

Looking now at the rising time τ_r^+, it increases also significantly and non linearly downstream. At the first two stations, the friction gain reached is quite comparable and the rising time is not very different (as illustrated by the curves of figure 8(a)). At the last station, the gain in friction is much less and the rising time is much larger. This means that when moving downstream, the control vortices encounter more difficulty to modify the wall region and need more time to do it. The lower is the friction gain, the longer is the time needed to reach stability. Besides, as figure 9 shows a significant spanwise modulation of the wall friction and rising time under control (which is recalled in table 2 for $X/H_s = 0.49$), another possible explanation to the downstream increase of τ_r^+ is the spanwise migration by self induction of the co-rotating vortical system generated by the actuators when progressing downstream.

For the pulsed actuation case studied here in detail, there is a strong modulation of the wall friction (as illustrated by figure 7). The determination of t_d^+ and τ_r^+ is consequently more difficult especially at

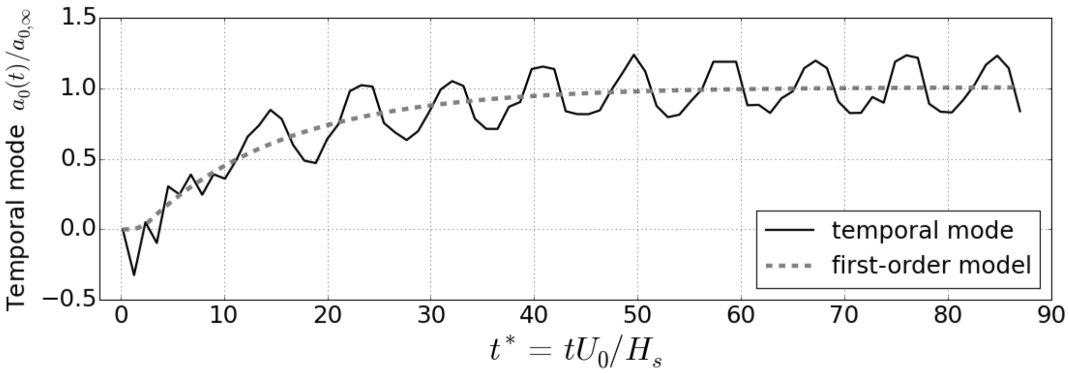

Fig. 15 Evolution in time of the temporal mode $a_0(t)/a_{0,\infty}$ (black line) and first-order model with delay fitted on this mode (grey dashed line). The corresponding characteristic time is $\tau_r^+ = \tau_r U_0/L_{sep} = 4.1$.

the downstream stations. At $X/H_s = 0.49$, which is illustrated in figure 7, values of 1.2 and 11.7 are found for these two parameters respectively. This is understandable: the control flow reaches the sensor at the same time for both continuous and pulsed blowing as mostly convection is involved at this upstream position. When the signal starts to rise, it takes nearly twice as much time to reach a stable state in the pulsed case as the actuation strength varies significantly due to pulsation and operates on average half the time with a the duty cycle of 50%. A careful comparison of the PIV data in Raibaudo (2015) shows that the separation point moves at nearly the same speed along the wall in the two cases. So t_d^+ should be comparable. As the actuation is operating only half of the time, it is expected that the rising time is also significantly increased at stations $SX2$ and $SX3$.

As can be seen, the effect of pulsing the actuation not only reduces the efficiency of the control compared to continuous blowing but affects also the dynamical response.

Table 3 gathers the data obtained in the present study on the reattachment rising time τ_r^+ from the analysis of the phase averaged PIV data. These data are ordered from the most global to the most local criterion and compared to relevant results from the literature. It should be reminded that the data presented were obtained in the streamwise/wall normal plane, midway between two actuators (thanks to the spanwise periodicity).

The rising time of the first CPOD coefficient $a_0(t)$ is representative of the global response of the flow, as it is obtained by averaging information over the whole PIV field. It appears to be the shortest one. The rising time based on the separation bubble length, obtained from the same PIV data, but which is more representative of what happens near the wall, is slightly longer (4.8 instead of 4.1). This second parameter should be looked at with caution because figure 10 has shown that, in the stabilized state, a new separation bubble creates itself upstream while the previous one disappears downstream. Also, the fit of a first order model on the curve of figure 13b is not straightforward. As was seen just above, the rising time of the wall friction itself is clearly much longer. At $X/H_s = 0.49$, it is already nearly 3 times longer than for $a_0(t)$. Consequently, if the outer flow appears to respond quite rapidly to the control, the near wall region needs much more time to stabilize and this more and more when moving downstream and when the established skin friction gain decreases.

For comparison, two experiments from the literature described in the introduction, which are not too far from the present one in terms of flow geometry were retained. Darabi and Wygnanski (2004) did study the separation over a plane flap placed at a large enough angle to a stream-aligned flat plate to have a massive separation. The control was performed using a spanwise slot at the articulation between the flat plate and the flap, feeded by a loud speaker to generate a pulsating control. The parameter used to characterize the time response of the system was the normal force coefficient to the flap. Mathis et al (2009) did their study on a bevelled trailing edge. The flow was controlled using again a spanwise slot

Present study	τ_r^+	4.1	CPOD mode $a_0(t)$
		4.8	Separation length
		11.7	Friction gain
Literature	t_r^+	16.	Darabi and Wygnanski (2004) Normal force coefficient
		4.7	Mathis et al (2009) Conditional POD

Table 3 Characteristic times obtained from different criteria in the pulsed actuation case compared with results from the literature.

at the geometric singularity, but this time with compressed air and an electrovalve to pulse the flow. The criterion used to characterize the transient behavior was comparable to the POD one used here. A Bi-Orthogonal decomposition (BOD) was performed on PIV data in the near wake of the splitter plate. These two contributions have a different definition of the characteristic time and a different scaling. Darabi and Wygnanski (2004) use the time to reach the steady state of the attached flow and scale it with the freestream velocity and the flap length. Mathis et al (2009) fit an exponential to the BOD chronos (they look mostly at the first and third chronos) and use the coefficient of the exponent, which is somehow closer to the present approach. They scale the time with the freestream velocity and the length of the bevel. Based on the fact that the separation length used here as length scale is relatively close to the length of the flap, it is not excessive to consider that the scaling is more or less the same in these three studies. Concerning their definition, the characteristic times obtained by Darabi and Wygnanski (2004) should be longer. Looking for example at figure 7, such a definition gives $t_r^* \simeq 140$ that is $t_r^+ \simeq 40$ compared to $\tau_r^+ = 11.7$ obtained here. Looking at table 3, the characteristic time of Darabi and Wygnanski (2004) is effectively larger by a factor of about 4 compared to the present POD result. Concerning Mathis et al (2009), the definition is different but similar and the characteristic time obtained is fairly close to the present result. The extra information brought by the present study, thanks to the wall friction measurements (and beside a refined characterization of the flow reattachment process), is that near the wall the flow needs more time to reach a steady state and increasingly when the final wall friction reached decreases.

One interesting question is whether this conclusion can be generalized further? For example to the control of wing profiles separation. Looking at the work of Amitay and Glezer (2002) and Siauw (2008) which are representative of this configuration, it is clear that the effect of the control on the circulation around the airfoil changes significantly the physics of the attachment process. Significant transverse vortices (similar to a starting vortex) are generated just after the onset of the actuation which are not evidenced here. Also, the length scale used in these studies is the cord of the model, which is significantly shorter than the size of the initial separated region. Such comparisons need consequently further studies.

As can be seen, despite the difference in geometry and in actuation strategy, when scaled with the freestream velocity and a length which is more or less representative of the streamwise extent of the separation region, there is a fairly good agreement on the characteristic time of global reattachment between the three studies of table 3. The results show that the separation over a ramp or flap type of geometry could be considered as first order dynamical system with a rising time τ_r^+ of the order of 4 to 5. It is interesting to note that in the case of Mathis et al (2009) the ratio of the upcoming boundary layer thickness to the separation region size is comparable to the present study while for Darabi and Wygnanski (2004) this ratio is probably smaller (although not given). Also, the Reynolds number is quite different between the three studies, the present one being significantly higher. This enlarges somehow the universality of the present conclusion and confirms the statement of Darabi and Wygnanski (2004) that the flow behavior is "almost independent of the upstream boundary-layer thickness and the global Reynolds number".

Conclusions

The dynamics of the control of a separated flow over a ramp model at high Reynolds number using continuous and pulsed vortex generators jets was investigated in the present study. The objective was to establish the characteristic times of the reattachment dynamics through different measurement techniques. The separated flow was characterized using PIV measurements. A massive separation bubble of $3.4H_s$ in length was identified using the backflow criteria (Simpson (1989)). A large region of high turbulent kinetic energy was observed downstream the ramp above the separation bubble.

The transient dynamics of the flow between separated and attached flow was first studied with continuous blowing using hot-film sensors distributed on the flap. The transition of the phase-averaged friction gain $E(t) - E_0$ during the reattachment can be modeled with a first-order response with delay. This is also true for pulsed actuation but with oscillations around the model and the final mean value. Characteristic times for reattachment $\tau_r^+ = \tau_r\ U_0\ /\ L_{sep} = 11.7$ and separation $\tau_s^+ = \tau_s\ U_0\ /\ L_{sep} = 9.4$ were estimated from the first-order model for the pulsed case considered. They are in agreement with previous studies (Amitay and Glezer (2002), Darabi and Wygnanski (2004), Mathis et al (2009)). At the most upstream sensor, the delay t_d can be explained by the convection of the actuation vortices. Downstream this delay increases non linearly and is linked to the displacement of the separation point on the flap during the reattachment process. The distribution of friction gain on the flap provides evidences of the three-dimensionality of the controlled flow. When the stationary reattachment is reached, the separated bubble is periodically pushed downstream and totally disappears at $\theta = (t^\star/T).360° = 99°$. A periodic emission of pockets of turbulence is observed, generated by thin shear layers originating from the leading edge of the flap and convected downstream. The dynamics of the reattachment under pulsed actuation was also studied through phase-averaged PIV velocity fields. For the first pulse, the separation bubble kept mostly its length during its downstream convection, but slightly flattens to the wall. A new bubble is then generated upstream, smaller and shorter in length compared to the baseline. The turbulent kinetic energy peak is reduced by 23 % and a high level of shear is observed at the flap leading edge. The second actuation pulse is nearly enough to lead the flow to its stabilized periodic attached regime.

A careful analysis of different characteristic times based on different tools (wall friction gain, separation length, conditional POD mode behavior) and a thorough comparison with the literature shows that despite significant differences in flow geometry and actuation strategies, a fairly good agreement arises on the characteristic time of the transient toward reattachment when scaled with the freestream velocity and a length scale representative of the streamwise extent of the separation bubble. A first-order dynamical system with a rising time $\tau_r^+ \simeq 4 - 5$ seems to be a reasonable model of the reattachment transient dynamics. It appears also that the conclusion of Darabi and Wygnanski (2004) that this transient is "almost independent of the upstream boundary layer thickness and the global Reynolds number" is confirmed by the precedent analysis.

Acknowledgments

The present work is supported by the Agence National de la Recherche (ANR) through the french ANR project SePaCode (ANR-11-BS09-0018) and by the CISIT International Campus through the Contraéro project. The authors are indepted to C. Cuvier for his help during the experiments and for the PIV images processing.

References

Amitay M, Glezer A (2002) Controlled transients of flow reattachment over stalled airfoils. International Journal of Heat and Fluid Flow 23(5):690–699, DOI 10.1016/S0142-727X(02)00165-0, URL http://linkinghub.elsevier.com/retrieve/pii/S0142727X02001650

Braud C, Dyment A (2012) Model of an impulsive subsonic jet actuator for flow control applications. Physics of Fluids 24(4), DOI 10.1063/1.3701377, URL http://scitation.aip.org/content/aip/journal/pof2/24/4/10.1063/1.3701377

Carlier J, Stanislas M (2005) Experimental study of eddy structures in a turbulent boundary layer using particle image velocimetry. Journal of Fluid Mechanics 535:143–188, DOI 10.1017/S0022112005004751, URL http://www.journals.cambridge.org/abstract{_}S0022112005004751

Chabert T, Dandois J, Garnier E, Jacquin L (2013) Experimental detection of a periodically forced turbulent boundary layer separation. Experiments in Fluids 54(2), DOI 10.1007/s00348-012-1430-1, URL http://link.springer.com/10.1007/s00348-012-1430-1

Chun KB, Sung HJ (1996) Control of turbulent separated flow over a backward-facing step by local forcing. Experiments in Fluids 21(6):417–426, DOI 10.1007/BF00189044, URL http://link.springer.com/10.1007/BF00189044

Compton DA, Johnston JP (1992) Streamwise vortex production by pitched and skewed jets in a turbulent boundary layer. AIAA Journal 30(3):640–647, DOI 10.2514/3.10967, URL http://arc.aiaa.org/doi/abs/10.2514/3.10967

Cuvier C (2012) Active control of a separated turbulent boundary layer in adverse pressure gradient. PhD thesis, École Centrale de Lille

Cuvier C, Foucaut J, Braud C, Stanislas M (2014) Characterisation of a high Reynolds number boundary layer subject to pressure gradient and separation. Journal of Turbulence 15(8):473–515, DOI 10.1080/14685248.2014.914217, URL http://dx.doi.org/10.1080/14685248.2014.914217

Darabi A, Wygnanski I (2004) Active management of naturally separated flow over a solid surface. Part 1. The forced reattachment process. Journal of Fluid Mechanics 510:105–129, DOI 10.1017/S0022112004009231, URL http://www.journals.cambridge.org/abstract{_}S0022112004009231http://journals.cambridge.org/abstract{_}S0022112004009231

Foucaut JM, Coudert S, Braud C, Velte C (2014) Influence of light sheet separation on SPIV measurement in a large field spanwise plane. Measurement Science and Technology 25, DOI 10.1088/0957-0233/25/3/035304, URL http://stacks.iop.org/0957-0233/25/i=3/a=035304?key=crossref.008464304c584e84d84c30b49c6870ef

Gautier N, Aider JL (2014) Feed-forward control of a perturbed backward-facing step flow. Journal of Fluid Mechanics 759:181–196, DOI 10.1017/jfm.2014.518, URL http://www.journals.cambridge.org/abstract{_}S0022112014005187

Godard G, Stanislas M (2006) Control of a decelerating boundary layer. Part 3: Optimization of round jets vortex generators. Aerospace Science and Technology 10(6):455–464, DOI 10.1016/j.ast.2005.11.005, URL http://www.sciencedirect.com/science/article/pii/S1270963805001616http://linkinghub.elsevier.com/retrieve/pii/S1270963805001616

Godard G, Foucaut JM, Stanislas M (2006) Control of a decelerating boundary layer. Part 2: Optimization of slotted jets vortex generators. Aerospace Science and Technology 10(6):455–464, DOI 10.1016/j.ast.2005.11.005, URL http://linkinghub.elsevier.com/retrieve/pii/S1270963805001628http://www.sciencedirect.com/science/article/pii/S1270963805001616http://linkinghub.elsevier.com/retrieve/pii/S1270963805001616

Gad-el hak M (2000) Flow control: passive, active and reactive flow management, cambridge edn

Hasan MAZ (1992) The flow over a backward-facing step under controlled perturbation: laminar separation. Journal of Fluid Mechanics 238:73–96, DOI 10.1017/S0022112092001642, URL http://www.journals.cambridge.org/abstract{_}S0022112092001642http:

//journals.cambridge.org/abstract{_}S0022112092001642

Kerstens W, Pfeiffer J, Williams D, King R, Colonius T (2011) Closed-Loop Control of Lift for Longitudinal Gust Suppression at Low Reynolds Numbers. AIAA Journal 49(8):1721–1728, DOI 10.2514/1.J050954

Kostas J, Foucaut JM, Stanislas M (2007) The flow structure produced by pulsed-jet vortex generators in a turbulent boundary layer in an adverse pressure gradient. Flow, Turbulence and Combustion 78:331–363, DOI 10.1007/s10494-007-9069-3, URL http://link.springer.com/10.1007/s10494-007-9069-3

Lögdberg O (2008) Turbulent boundary layer separation and control. PhD thesis, KTH, URL http://kth.diva-portal.org/smash/record.jsf?pid=diva2:133356

Marquillie M, Ehrenstein U (2003) On the onset of nonlinear oscillations in a separating boundary-layer flow. Journal of Fluid Mechanics 490:169–188, DOI 10.1017/S0022112003005287, URL http://www.journals.cambridge.org/abstract{_}S0022112003005287

Mathis R, Lebedev A, Collin E, Delville J, Bonnet JP (2009) Experimental study of transient forced turbulent separation and reattachment on a bevelled trailing edge. Experiments in Fluids 46(1):131–146, DOI 10.1007/s00348-008-0549-6, URL http://link.springer.com/10.1007/s00348-008-0549-6

McManus K, Legner H, Davis S (1994) Pulsed vortex generator jets for active control of flow separation. In: AIAA paper, American Institute of Aeronautics and Astronautics, Colorado Springs, USA, DOI 10.2514/6.1994-2218, URL http://arc.aiaa.org/doi/pdf/10.2514/6.1994-2218

Milanovic IM, M Q Zaman KB (2004) Fluid Dynamics of Highly Pitched and Yawed Jets in Crossflow. AIAA Journal 42(5):874–882, DOI 10.2514/1.2924

Nakayama A, Stack JP, Lin JC, Valarezo WO (1993) Surface hot-film method for the measurement of transition, separation and reattachment points. AIAA 24th Fluid Dynamics, Plasmadynamics, and Lasers Conference, 0rlando, USA URL http://adsabs.harvard.edu/abs/1993fldy.conf.....N

Ortmanns J, Bitter M, Kähler CJ (2008) Dynamic vortex structures for flow-control applications. Experiments in Fluids 44(3):397–408, DOI 10.1007/s00348-007-0442-8, URL http://link.springer.com/10.1007/s00348-007-0442-8

Raibaudo C (2015) Characterization of the transient of a separated turbulent boundary layer under control and applications to advanced closed-loop controllers. PhD thesis, École Centrale de Lille

Selby GV, Lin JC, Howard FG (1992) Control of low-speed turbulent separated flow using jet vortex generators. Experiments in Fluids 12(6):394–400, DOI 10.1007/BF00193886, URL http://link.springer.com/article/10.1007/BF00193886http://link.springer.com/10.1007/BF00193886

Shaqarin T (2011) Closed-loop active separation control. PhD thesis, Université de Lille 1

Shaqarin T, Braud C, Coudert S, Stanislas M (2013) Open and closed-loop experiments to identify the separated flow dynamics of a thick turbulent boundary layer. Experiments in Fluids 54(2):1448, DOI 10.1007/s00348-012-1448-4, URL http://link.springer.com/10.1007/s00348-012-1448-4

Siauw W (2008) Transient process of separation and attachment over a NACA 0015 airfoil controlled by fluidic vortex generators. PhD thesis, Université de Poitiers, URL http://www.theses.fr/2008POIT2313

Simpson RL (1989) Turbulent boundary layer separation. Annual Review of Fluid Mechanics 21:205–234, DOI 10.1016/0376-0421(95)00012-7

Stalnov O, Palei V, Fono I, Cohen K, Seifert A (2007) Experimental estimation of a D-shaped cylinder wake using body-mounted sensors. Experiments in Fluids 42(4):531–542, DOI 10.1007/s00348-007-0255-9, URL http://link.springer.com/10.1007/s00348-007-0255-9

Tilmann C, Langan K, Betterton J, Wilson M (2006) Characterisation of pulsed vortex generator jets for active flow control. Symposium on "Active Control Technology" for Enhanced Performance Operational Capabilities of Military Aircraft, Land Vehicles and Sea Vehicles URL http://oai.dtic.mil/oai/oai?verb=getRecord{&}metadataPrefix=html{&}identifier=ADA418147

Woo GTK, Crittenden T, Glezer A (2009) Transitory separation control over a stalled airfoil. In: 39th AIAA Fluid Dynamics Conference, American Institute of Aeronautics and Astronautics, San Antonio, USA, DOI 10.2514/6.2009-4281, URL http://arc.aiaa.org/doi/pdf/10.2514/6.2009-4281